A T-spline-based approach for interface debonding using cohesive zone models

A T-spline-based approach for interface debonding using cohesive zone models

Rossana Dimitri[1], Laura De Lorenzis[2], Giorgio Zavarise[1]

[1]*Dipartimento di Ingegneria dell'Innovazione, Università del Salento, Italy*
E-mail: rossana.dimitri@unisalento.it, giorgio.zavarise@unisalento.it

[2]*Institut für Angewandte Mechanik, Technische Universität Braunschweig, Germany*
E-mail: l.delorenzis@tu-braunschweig.de

Keywords: Cohesive zone modeling, contact mechanics, isogeometric analysis, T-splines.

SUMMARY. Cohesive zone (CZ) models have long been used by the scientific community to analyze the progressive damage of materials and interfaces. Based on these models, non-linear relationships between tractions and relative displacements are assumed. These relationships dictate both the work of separation per unit fracture surface and the peak stress that has to be reached for the crack formation. This contribution deals with T-spline-based isogeometric CZ modeling of interface debonding, where the path of the debonding crack is known *a priori*. The interface is discretized with zero-thickness contact elements which account for both contact and debonding within a unified framework, using a Gauss-point-to-surface formulation. Depending on the contact status, an automatic switching procedure is used to choose between cohesive and contact models. The continuum is discretized with cubic T-splines, as well as with cubic Non Uniform Rational B-Splines (NURBS) and Lagrange polynomial elements for comparison purposes. Results for the double cantilever beam test and for the peel test with varying resolutions of the process zone and varying number of Gauss points used for the enforcement of the contact constraints are presented and compared. The superior accuracy of T-splines interpolations with respect to the NURBS and Lagrange ones for a given number of degrees of freedom is verified.

1 INTRODUCTION

Interfacial debonding often results in failure of laminated or generally jointed structures. Different numerical approaches have been proposed in the literature for the simulation of this process. Due to the appealing feature of predicting both the debonding onset and its growth, cohesive zone models (CZMs) have been widely used as numerical tool to simulate debonding as a result of the progressive decay of cohesive forces and the formation of traction-free surfaces between two materials or laminated structures where the potential cracks are known a priori [1,2].

The numerical application of CZMs for debonding problems within finite element frameworks suffers from an intrinsic discretization sensitivity. Unless a sufficiently fine mesh discretizes the process zone of a cohesive crack, a sudden release of energy in large cohesive zone elements causes a sequence of artificial (non physical) snap-through or snap-back points in the global load-deflection response, thus compromising the numerical efficiency [3]. Such situations lead to major numerical difficulties in solving the global system of equations, due to the fact that a standard Newton-Raphson iterative scheme fails to converge in the case of snap-backs or snap-through. A current solution strategy with respect to this problem aims at eliminating or reducing the oscillations. Since the observed oscillations are discretization-induced, they are alleviated through

mesh refinement. In contrast to refinement of the entire domain, local refinement of the process zone is a computationally more efficient alternative. To this end, different surface enrichment strategies have been developed in the literature using different types of enrichment functions for CZ interface elements [3,4], as well as for contact elements [5]. These techniques, however, only affect the interacting surfaces and leave the bulk behavior of the solid unaltered. Moreover, they typically do not increase the degree of continuity of the parameterization at the inter-element boundaries which is also responsible for unphysical stress oscillations at the interface.

The isogeometric analysis (IGA) framework [6] has already demonstrated to guarantee substantial advantages in the computational treatment of unilateral contact by applying both NURBS and T-Splines [7-9]. The contact pressure distributions stemming from NURBS parameterizations are always non-negative and are virtually insensitive to changes in the interpolation order. In contrast, higher-order Lagrange parameterizations are sensitive to interpolation order, often display spurious oscillations, and may attain significant unphysical negative values. Moreover, for contact between smooth bodies the higher continuity achieved by the isogeometric discretization eliminates the need for special treatment of corner/edge cases or normal averaging procedures and enhances iterative convergence and robustness in the solution of the non-linear problem.

As a design tool NURBS, surfaces are limited by the simple fact that they are four sided, and their control mesh consists of a tensor product grid of control points. In the context of refinement this means that adding new control points to a NURBS surface entails adding entire rows or columns of control points to maintain this tensor product structure. Differently from NURBS, T-splines allow local refinement due to the introduction of T-junctions and extraordinary points [10]. The T-Spline-based isogeometric approach is particularly suitable for CZ modeling, due to the high resolution required by these models in the process zone. Furthermore, in the isogeometric setting the discretized crack surfaces feature higher order inter-element continuity with respect to classical finite elements. In this contribution, debonding problems at known interfaces are treated with CZ modeling within the T-spline-based isogeometric framework, from which the NURBS framework can be recovered as a special case. The T-spline-based discretization is developed from the finite element point of view, using the Bézier extraction. The idea is to extract the linear operator which maps the Bernstein polynomial basis on Bézier elements to the global T-spline basis. In this way the isogeometric discretizations are automatically generated for any analysis-suitable CAD geometry and easily incorporated into existing finite element frameworks [9,10]. A commercial T-spline plugin has been introduced recently for Rhino3d by Autodesk which is capable of defining and exporting analysis-suitable T-spline models (based on Bézier extraction) for use in IGA. This plugin is used to build the T-spline analysis models adopted in this study from a finite element point of view.

2 NUMERICAL MODEL

2.1 *Isogeometric analysis: T-splines fundamentals*

In this section, the T-splines technology is briefly reviewed. We refer to [10] for details. In what follows we focus on cubic T-splines surfaces due to their predominance in industry. The spatial and parametric dimensions is denoted by d_s and d_p, respectively. We denote also an element index by e and the number of non-zero basis functions over an element e by n. An important object of interest underlying T-spline technology is the T-mesh. For surfaces, a T-mesh is a polygonal mesh and we will refer to the constituent polygons as elements or, equivalently, faces.

Each element is a quadrilateral whose edges are permitted to contain T-junctions – vertices that are analogous to hanging nodes in finite elements. A control point, $\mathbf{P}_A \in \Re^{ds}, d_s = 2$ and control weight $w_A \in \Re$ where the index A denotes a global control point number, is assigned to every vertex in the T-mesh. The valence of a vertex is the number of edges that touch the vertex. An extraordinary point is an interior vertex that is not a T-junction and whose valence does not equal four. Figure (1) shows an unstructured T-mesh. Notice the valence three and valence five extraordinary points denoted by open circles. The single T-junction is denoted by an open square.

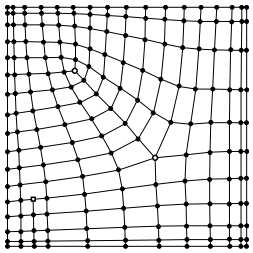

Figure 1: An unstructured T-mesh. Extraordinary points are denoted by open circles and T-junctions are denoted by open squares.

In this paper, we develop T-splines from the finite element point of view, utilizing Bézier extraction. The idea is to extract the linear operator which maps the Bernstein polynomial basis on Bézier elements to the global T-spline basis. The linear transformation is defined by a matrix referred to as the extraction operator and denoted by $\mathbf{C}^e$. The transpose of the extraction operator maps the control points of the global T-spline to the control points of the Bernstein polynomials. Figure 2 illustrates the idea for a B-spline curve.

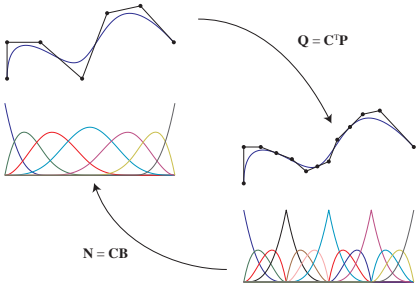

Figure 2: Schematic representation of Bézier extraction for a B-spline curve. B-spline basis functions and control points are denoted by $\mathbf{N}$ and $\mathbf{P}$, respectively. Bernstein polynomials and control points are denoted by $\mathbf{B}$ and $\mathbf{Q}$, respectively. The curve $T(\xi) = \mathbf{P}^T\mathbf{N}(\xi) = \mathbf{Q}^T\mathbf{B}(\xi)$.

This provides a finite element representation of T-splines, and facilitates the incorporation of T-splines into existing finite element programs. Only the shape function subroutine needs to be modified. All other aspects of the finite element program remain the same. Based on the isoparametric approach, the unknown displacement field, its variation and the coordinates in the current configuration over a contact element have been defined as follows

$$\mathbf{u}^e(\xi) = \sum_{a=1}^{n} R_a^e(\xi)\mathbf{u}_a^e \quad \delta\mathbf{u}^e(\xi) = \sum_{a=1}^{n} R_a^e(\xi)\delta\mathbf{u}_a^e \quad \mathbf{x}^e(\xi) = \sum_{a=1}^{n} R_a^e(\xi)\mathbf{x}_a^e \quad , \tag{1}$$

where $\mathbf{u}_a^e$, $\delta\mathbf{u}_a^e$ and $\mathbf{x}_a^e$ are the unknown displacement, displacement variation, and current coordinate of the control point $\mathbf{P}_A$, respectively, $A = IEN(a,e)$ is a mapping from the local element numbering to the global control point numbering, and $R_a^e(\xi)$ is the generic rational T-spline basis function pertaining to element e. Note that $\mathbf{x}_a^e = \mathbf{X}_a^e + \mathbf{u}_a^e$.

2.2 *Gauss-point-to-surface (GPTS) contact and debonding algorithm*

In this work, the interface is discretized with zero-thickness contact elements which account for both contact and debonding within a unified framework, using a Gauss-point-to-surface formulation as proposed in [11]. The algorithm has been here implemented in the finite element code FEAP (courtesy of Prof. R.L. Taylor) for NURBS and T-Splines discretizations. This formulation is characterized by the independent enforcement of the contact constraints at each quadrature point associated with the frictionless contact contribution to the virtual work. The virtual variation of the contact contribution to the potential is expressed as

$$\delta W_c = \int_{\Gamma_c} p_N \, \delta g_N \, d\Gamma, \tag{2}$$

where the integral is evaluated on the pull-back of the active contact region in the reference configuration, Γ_c, through the use of an active set strategy. In eq. (2), p_N denotes the normal cohesive or contact force, and g_N is the normal gap between the two bodies in contact, one of which is taken as 'slave' and the other as 'master'. The gap can be expressed as follows

$$g_N = \left(\mathbf{x}^s - \mathbf{x}^m\right) \cdot \mathbf{n}, \tag{3}$$

In eq. (3), $\mathbf{n} = \mathbf{n}^m$ is the outward normal unit vector to the master surface, while $\mathbf{x}^s, \mathbf{x}^m$ represent the current positions of a point of the slave body, and of its closest-point projection on the master body, respectively. With this definition, for positive g_N cohesive forces arise, and for negative g_N penetration between the bodies takes place and the contact algorithm is activated. The non-penetration condition is here enforced in the normal direction using the penalty method. Depending on the gap status, an automatic switching procedure is thus used to choose between cohesive and contact models. The resulting non-linear problem is solved with a Newton-Raphson procedure. The global tangent stiffness matrix is obtained with a consistent linearization of eq. (2). Such a linearization yields

$$\Delta\delta W_c = \int_{\Gamma c} \frac{\partial p_N}{\partial g_N} \Delta g_N \, \delta g_N \, d\Gamma + \int_{\Gamma c} p_N \Delta\delta g_N d\Gamma, \tag{4}$$

where the symbols δ and Δ denote, respectively, virtual variation and linearization. The geometrical parameters δg_N and $\Delta\delta g_N$ are determined based on the contact T-spline element geometry as

$$\delta g_N = \delta\mathbf{u}^T\mathbf{N} \quad \Delta g_N = \mathbf{N}^T\Delta\mathbf{u} \quad , \tag{5}$$

where the following vectors have been defined

$$\delta\mathbf{u} = \begin{bmatrix} \delta\mathbf{u}_1^s \\ \vdots \\ \delta\mathbf{u}_{n^s}^s \\ \delta\mathbf{u}_1^m \\ \vdots \\ \delta\mathbf{u}_{n^m}^m \end{bmatrix} \quad \Delta\mathbf{u} = \begin{bmatrix} \Delta\mathbf{u}_1^s \\ \vdots \\ \Delta\mathbf{u}_{n^s}^s \\ \Delta\mathbf{u}_1^m \\ \vdots \\ \Delta\mathbf{u}_{n^m}^m \end{bmatrix} \quad \mathbf{N} = \begin{bmatrix} R_1^s(\xi_s)\mathbf{n} \\ \vdots \\ R_{n^s}^s(\xi_s)\mathbf{n} \\ -R_1^m(\xi_m)\mathbf{n} \\ \vdots \\ -R_{n^m}^m(\xi_m)\mathbf{n} \end{bmatrix}, \tag{6}$$

In eq. (6) n^s and n^m are the number of basis functions having support on the element of the slave and master body, respectively, where the quantities are currently being evaluated; ξ_s are the parametric coordinates of the point on the slave surface where the quantities are being evaluated, and ξ_m are the parametric coordinates of the respective projection point on the master surface. The normal traction forces p_N as well as their partial derivatives with respect to the normal relative displacements $\partial p_N / \partial g_N$ depend on the cohesive or contact law parameters. By substitution of eq. (5) in eq. (2), the cohesive or contact contribution to the residual vector for the Newton-Raphson iterative solution of the non-linear problem is obtained as

$$\mathbf{R} = \int_{\Gamma c} p_N \mathbf{N} d\Gamma, \tag{7}$$

For positive gaps, a bilinear cohesive zone law is here considered whose simple shape is able to capture the main characteristic parameters of interfaces, i.e. the cohesive strength, $P_{n,max}$, the critical value of the normal relative displacement, g_{Nu}, as well as the linear-elastic properties (slope of the curve in the ascending branch). For the law chosen in this study, it is (see also Figure 3)

$$\frac{\partial p_N}{\partial g_N} = \begin{cases} \varepsilon_N & for \quad g_N < 0 \\ \dfrac{p_{N\max}}{g_{N\max}} & for \quad 0 \le g_N < g_{N\max} \\ \dfrac{-p_{N\max}}{g_{Nu} - g_{N\max}} & for \quad g_{N\max} \le g_N < g_{Nu} \end{cases}, \tag{8}$$

where ε_N is the penalty parameter.

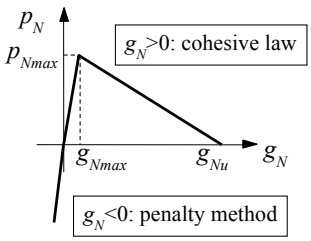

Figure 3: Interfacial tractions-relative displacements law in the normal direction.

3 NUMERICAL RESULTS

3.1 *Numerical examples*

Two examples involving large deformations in plane stress conditions are now presented to demonstrate the accuracy and quality of the proposed contact and debonding formulation. For comparison purposes, not only T-splines but also NURBS and Lagrange discretizations are employed. The generation of the geometry and refinement are first conducted on the exact T-spline parameterization, where T-junctions are locally added in the meshes near the contact surfaces, and then converted to the NURBS and Lagrange parameterizations, for the same global number of degrees of freedom (D_0).

As first example, we consider the classical mode-I double cantilever beam (DCB) in plane stress, used in the ASTM3433 standard to determine the mode I fracture toughness. A specimen with length $L = 14mm$, width $w = 1mm$, thickness $h = 0.2mm$, and precrack length $a_0 = 4mm$, is gradually pulled apart in displacement control (Figure 4a). An elastic isotropic behavior is assumed for both master and slave bodies, with material properties $E = 120GPa$ and $\nu = 0.2$. The penalty parameter is $\varepsilon_N = 10^5$, and two Gauss points are considered for each element of the contact interfaces. The global results in terms of load-deflection response is evaluated by considering two different mesh refinements with $D_0 = 280$ and $D_0 = 1956$, respectively, such that the element size at the interface is always less than the length of the fracture process zone wherein the cohesive traction-separation law is defined and the energy is dissipated. The effect of the interfacial strength on the numerical results is then studied by considering two different interfacial strengths ($p_{N\max} = 4MPa$, and $p_{N\max} = 6MPa$ respectively), for a fixed critical energy $G_{IC} = 0.1N/mm$ and a fixed ratio between the ultimate and maximum opening displacements $g_{Nu}/g_{N\max} = 12.5$ (Figure 5a).

The second example consists of a peel test between a fiber-reinforced polymer strip with length $L_2 = 150mm$ and thickness $h_2 = 2mm$ adhering to a concrete substrate with length $L_1 = 120mm$ and thickness $h_1 = 10mm$. The strip is peeled off the substrate by applying a vertical displacement at the right boundary, as shown in Figure 4b. An elastic isotropic behavior is assumed for both the bodies, with material properties $E_1 = 5MPa$ and $\nu_1 = 0.2$ for the substrate and $E_2 = 250MPa$ and $\nu_2 = \nu_1$ for the strip. Plane stress conditions are considered. The cohesive parameters are here taken as $p_{N\max} = 6MPa$, $G_{IC} = 0.1N/mm$, $g_{Nu}/g_{N\max} = 10$ (see Figure 5b), and a quite fine mesh with a total number of degrees of freedom $D_0 = 3700$ is here adopted to discretize the specimen. The penalty parameter ε_N is set to 10^3, and two Gauss points are considered for each element of the contact interfaces.

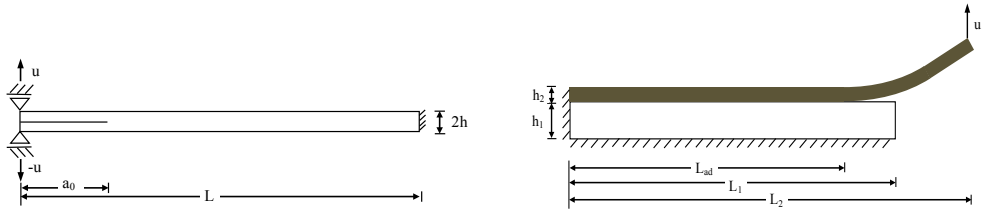

(a) (b)

Figure 4: The DCB (a) and the peel test (b) scheme.

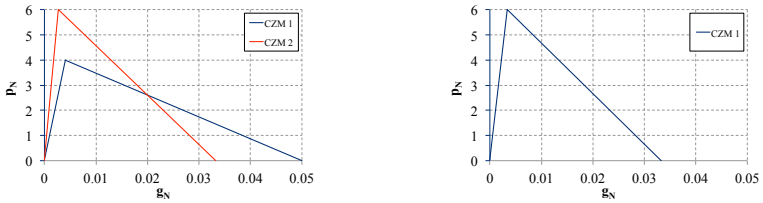

(a) (b)

Figure 5: Cohesive zone laws: the DCB test (a) and the peel test (b).

3.2 *The Double Cantilever Beam results*

Results for the DCB test with varying resolutions of the process zone are now presented for T-splines, NURBS and Lagrange discretizations with the same cubic polynomial order. In Figure 6, T-Splines interpolations are shown to outperform the NURBS and Lagrange interpolations for a given number of degrees of freedom. The solutions with T-splines feature significantly smaller oscillations during the entire debonding phase (i.e. in the softening branch of the curves) in comparison with NURBS and Lagrange solutions, thus reflecting the better ability of T-Splines to capture the debonding phenomena taking place in the process zone. This is due to their local refinement capability, and to the consequent better resolution of the interface for a given number of degrees of freedom. The worst results are always given by the Lagrange discretization. These results feature significant irregular oscillations in the debonding phase, due to the C^0 continuity at the inter-element boundaries as opposed to the C^2 continuity of both NURBS and T-Splines IGA basis functions.

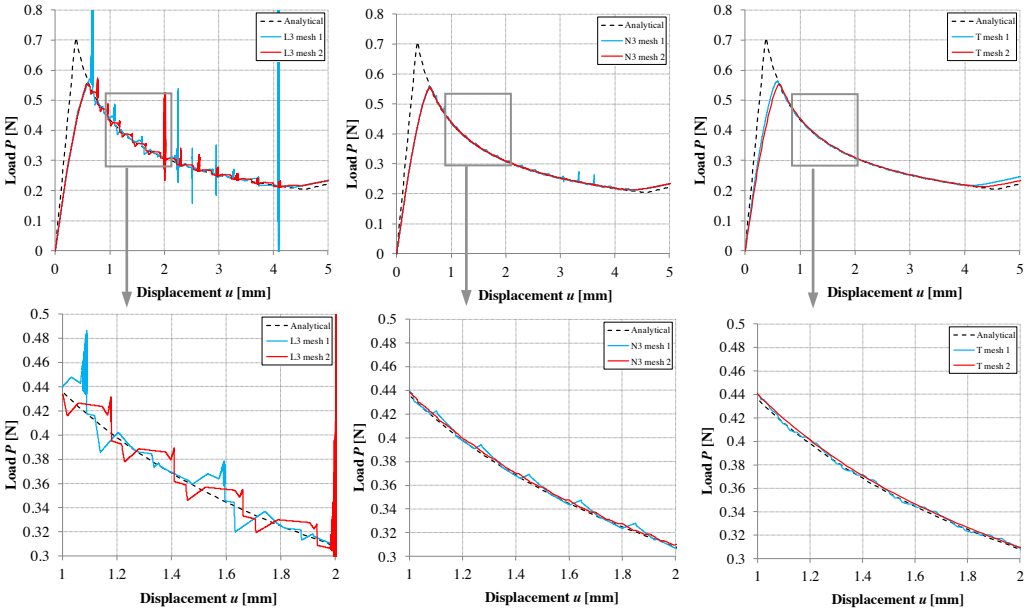

(a) Lagrange (b) NURBS (c) T-splines

Figure 6: Load-displacement curves for CZM 1. $\varepsilon_N = 10^5$ and $GP = 2$.

The effect of the increase of the interfacial strength is to reduce the length of the fracture process zone and therefore to decrease the number of elements spanning this zone. It is expected that if the fracture strength $p_{N\max}$ is increased to a point where less than one element spans the fracture process zone, convergence is no longer achieved or inaccurate results are found. For the limit case when $p_{N\max}$ tends to infinity, the size of the fracture process zone vanishes and the analytical solution based on elastic bending theory and linear elastic fracture mechanics (LEFM) becomes applicable. The LEFM curve is here considered for comparison purposes in all plots. By comparing Figures 6 and 7, it is evident as increasing the cohesive strength leads to more severe irregularities and oscillations in the global response both for Lagrange and NURBS discretizations. The process zone is localized in a smaller region spanning less elements, and a higher mesh resolution near the crack tip would be necessary to capture well the results. Also in this case, the T-spline global response is remarkably smooth and exhibits few oscillations with limited magnitude only for the coarsest analyzed mesh.

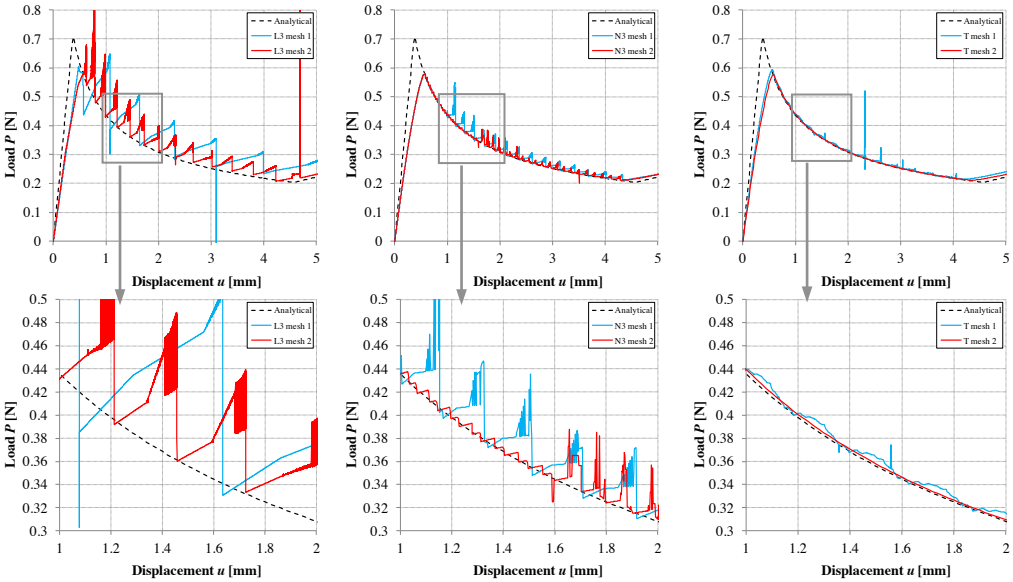

(a) Lagrange (b) NURBS (c) T-splines

Figure 7: Load-displacement curves for CZM 2. $\varepsilon_N = 10^5$ and $GP = 2$.

For completeness, the number of Gauss points (GP) where the contact constraints are enforced is varied in Figure 8 for the default penalty parameter $\varepsilon_N = 10^5$ and the highest $p_{N\max}$ here considered (i.e. for CZM 2). An increasing number of GP is beneficial as it improves the resolution in the computation of the cohesive or contact forces in the process zone and in its vicinity, especially for the coarsest meshes. This is evident both for Lagrange and NURBS discretizations, for which the magnitude of the oscillations is reduced for increasing GP, until macroscopically smooth curves are obtained. Conversely, the global response of T-spline discretizations is quite insensitive to the number of GP for the cohesive law here considered as a perfectly smooth curve is already obtained with only 2 GP.

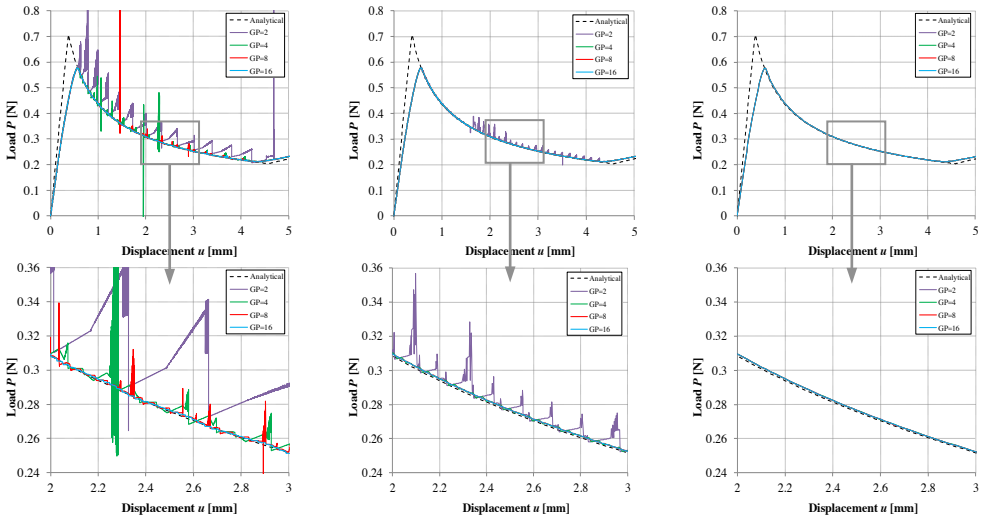

(a) Lagrange (b) NURBS (c) T-splines

Figure 8: Load-displacement curves for CZM 2. Effect of the number of Gauss points on each contact element. $\varepsilon_N = 10^3$.

3.1 *The peel test results*

The peel test in Figure 4b has been analyzed for varying adhesive length L_{ad} from 60mm up to 120mm. Figure 9 shows the computed global load-displacement curves of the peeling process for the three discretizations.

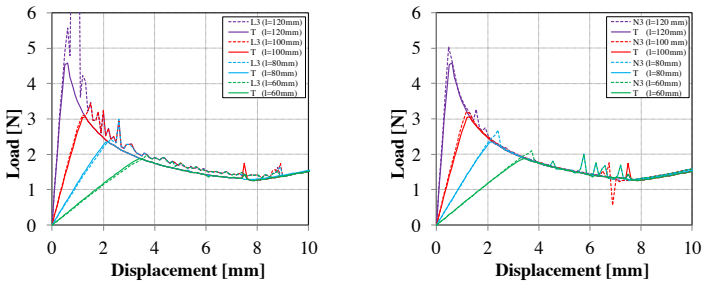

(a) Lagrange and T-splines (b) NURBS and T-splines

Figure 9: Load-displacement curves. $\varepsilon_N = 10^3$ and $GP = 2$.

The numerical curves are quite smooth for T-splines interpolations whereas they display significant oscillations both for NURBS and Lagrange interpolations in the softening stage. For each adhesive length here considered, the maximum load obtained with Lagrange or NURBS interpolations is larger than that given by T-splines. The oscillations strongly affect the convergence rate during the Newton-Raphson iteration used to solve the nonlinear problem. These oscillation errors are due to the poor discretization mesh at the contact surfaces both for Lagrange and NURBS. In contrast, the local refined T-spline mesh with T-junctions performs much better

and reduces the amplitude oscillations without increasing the computational cost.

4 CONCLUSIONS

This work evaluates the performance of T-splines-based isogeometric analysis for 2D mode-I debonding problems, as exemplified by a double-cantilever-beam and a bimaterial peel test. Based on the isogeometric concept in which the T-Splines representation of the bodies from CAD is maintained in a finite element environment, an integrated approach accounting for debonding and frictionless contact is implemented in the FEAP code for NURBS and T-Splines discretizations in 2D. A Gauss-point-to-surface formulation is adopted whereby a desired number of quadrature points is located on the contact surface and the contact/cohesive zone constraints are enforced independently at each of these points. The superior accuracy of T-spline interpolations with respect to the NURBS and Lagrange ones is proved by analyzing the global load-displacement curves for given number of degrees of freedom. This is due to the combined effect of the higher continuity achieved at the inter-element boundaries, the non-negativeness of the isogeometric basis functions, and the local T-spline refinement capability. The final outcome is that relatively coarse T-spline meshes (compared to the other types of interpolations) can be adopted for the analysis of debonding problems, thus reducing the computational expense, and accurate results with no visible oscillations in the global response curves can be obtained.

References

[1] Allix, O., and Ladeveze, P., "Interlaminar interface modelling for the prediction of delamination," *Compos. Struct.*, **22**, 235-242 (1992).

[2] Schellekens, J.C.J., and de Borst, R., "A non-linear finite element approach for the analysis of mode-i free edge delamination in composites," *Int. J. Solids Struct.*, **30**, 1239-1253 (1993).

[3] Criesfield, M.A., and Alfano, G., "Adaptive hierarchical enrichment for delamination fracture using a decohesive zone model," *Int. J. Numer. Meth. Engng.*, **54**, 1369-1390 (2002).

[4] Guimatsia, I., Ankersen, J.K., Davies, GAO, and Iannucci, L., "Decohesion finite element with enriched basis functions for delamination," *Composite Science and Technology*, **69(15-16)**, 2616-2624 (2009).

[5] Sauer, R., "Enriched contact finite elements for stable peeling computations," *Int. J. Numer. Meth. Engng.*, **87**, 593-616 (2011).

[6] Cottrell, J.A., Hughes, T.J.R., and Bazilevs, Y., "Enriched contact finite elements for stable peeling computations," *Int. J. Numer. Meth. Engng.*, **87**, 593-616 (2011).

[7] De Lorenzis, L., Temizer, I., Wriggers, P., and Zavarise, G., "A large deformation frictional contact formulation using NURBS-based isogeometric analysis," *Int. J. Numer. Meth. Engng.*, **87(13)**, 1278-1300 (2011).

[8] De Lorenzis, L., Wriggers, P., and Zavarise, G., "A mortar formulation for 3D large deformation contact using NURBS-based isogeometric analysis and the augmented Lagrangian method", *Comp. Mech.*, **49(1)**, 1-20 (2012).

[9] Dimitri, R., De Lorenzis, L., Scott, M.A., Wriggers, P., and Zavarise, G., "Isogeometric large deformation frictionless contact using T-splines," *submitted*

[10] Scott, M.A., Simpson, R.N., Evans, J.A., Lipton, S., Bordas, S.P.A., Hughes, T.J.R., and Sederberg, T.W., "Isogeometric boundary element analysis using unstructured T-splines," *Computer Methods in Applied Mechanics and Engineering*, **254**, 197-221 (2013).

[11] Fischer, K.A., and Wriggers, P., "Frictionless 2D contact formulations for finite deformations based on the mortar method," Computational Mechanics, **36**, 226–244 (2005).